Proceedings of the ASME-JSME-KSME 2011 Joint Fluids Engineering Conference
AJK-Fluids2011
July 24-29, 2011, Hamamatsu, Shizuoka, JAPAN

AJK2011-04001

A FULL EULERIAN FINITE DIFFERENCE METHOD FOR HYPERELASTIC PARTICLES IN FLUID FLOWS

Kazuyasu Sugiyama
Department of Mechanical Engineering, School of Engineering, The University of Tokyo
7-3-1, Hongo, Bunkyo-ku, Tokyo 113-8656, JAPAN

Satoshi Ii
Department of Mechanical Engineering, School of Engineering, The University of Tokyo
7-3-1, Hongo, Bunkyo-ku, Tokyo 113-8656, JAPAN

Shintaro Takeuchi
Department of Mechanical Engineering, School of Engineering, Osaka University
2-1 Yamda-oka, Suita, Osaka 565-0871, JAPAN

Shu Takagi
Department of Mechanical Engineering, School of Engineering, The University of Tokyo
7-3-1, Hongo, Bunkyo-ku, Tokyo 113-8656, JAPAN
Organ and Body Scale Team, CSRP, Riken
2-1, Hirosawa, Wako-shi, Saitama 351-0198, JAPAN

Yoichiro Matsumoto
Department of Mechanical Engineering, School of Engineering, The University of Tokyo
7-3-1, Hongo, Bunkyo-ku, Tokyo 113-8656, JAPAN

ABSTRACT

A full Eulerian finite difference method has been developed for solving a dynamic interaction problem between Newtonian fluid and hyperelastic material. It facilitates to simulate certain classes of problems, such that an initial and neutral configuration of a multi-component geometry converted from voxel-based data is provided on a fixed Cartesian mesh. A solid volume fraction, which has been widely used for multiphase flow simulations, is applied to describing the multi-component geometry. The temporal change in the solid deformation is described in the Eulerian frame by updating a left Cauchy-Green deformation tensor, which is used to express constitutive equations for incompressible hyperelastic materials. The present Eulerian approach is confirmed to well reproduce the material deformation in the lid-driven flow and the particle-particle interaction in the Couette flow computed by means of the finite element method. It is applied to a Poiseuille flow containing biconcave neo-Hookean particles. The deformation, the relative position and orientation of a pair of particles are strongly dependent upon the initial configuration. The increase in the apparent viscosity is dependent upon the developed arrangement of the particles.

INTRODUCTION

Numerical simulations of Fluid-Structure Interaction (FSI) problems would make it possible to predict the effect of a medical treatment and help one decide the treatment strategy in clinical practice. In particular, a blood flow simulation is expected to contribute to assisting the surgical planning of a cardiovascular disease and a brain aneurysm. Recently, there are growing expectations for its applications along with a progress in imaging and computational technologies. It is also expected to contribute to the field of life science, such as in the understanding of the very essence of life and the demonstration of pathological mechanisms. It is of great importance to develop numerical techniques suitable for the characteristics of body tissues, which are flexible and complicated in shape, when attempting to rationalize and to generalize the fluid-structure coupled analyses. The expectations include the further understandings of the micro/mesoscopic behavior of the flexibly deformable Red Blood Cells (RBCs) in plasma useful for evaluating the macroscopic blood rheology, and the thrombosis formation as aggregation of platelets, of which the

Copyright © 2011 by JSME

Downloaded From: https://proceedings.asmedigitalcollection.asme.org on 06/30/2019 Terms of Use: http://www.asme.org/about-asme/terms-of-use

motion is remarkably affected by the RBC inducing a transverse fluid fluctuation.

As in the case of industrial products, if a given blueprint can provide precise information on the boundary shape, the generation of meshes can be easily automated in many cases and accurate computations can be performed. However, a blueprint does not exist for the human body, and it therefore requires the acquisition of the multi-component geometric data converted from CT/MRI medical images before the mesh generation. The basic idea of the medical image-based simulation is found in [1, 2] dealing with blood flows in arteries. To predict the motion of moving/deforming objects, a finite element method based on an interface-tracking approach using a body-fit Lagrangian mesh, which includes Arbitrary Lagrangian Eulerian (ALE) [3, 4] and Deforming-Spatial-Domain/Space-Time (DSD/ST) [5, 6] methods, attains a highly accurate computation. An Eulerian-Lagrangian approach such as Immersed Boundary (IB) [7, 8] and Immersed Finite Element (IFE) [9] methods, in which the fluid and solid phases are separately formulated on the fixed Eulerian and Lagrangian grids, respectively, is also feasible and effective for the purpose. The ALE, DSD/ST, IB, and IFE approaches have been applied to a wide variety of biological problems. However, if the finite element is used for the analysis of a system involving complicated geometry of solid and/or a large number of objects, it requires not only a high computational cost but also a great effort to reconstruct the mesh at each time step when the medical image is converted into voxel data. As pointed out in [10, 11], technical knowledge and expertise are required for the mesh generation and reconstruction. To release the FSI simulation from the mesh distortion and/or the mesh reconstruction procedure, and to extend the applicability to certain additional classes of problems, full Eulerian approaches [12–19] and particle-in-cell approaches [20,21] have been explored.

The authors formulated the basic equations suited for monolithically treating the moving boundary kinematics and the dynamics in interaction between Newtonian fluid and hyperelastic material [18]. The numerical treatment is similar to the Volume-Of-Fluid (VOF), level-set or front-tracking method frequently applied to two-phase flow problems, namely, though the grid resolution is high enough to capture the interfacial profile, the grid system is not boundary-fit but rectangular. In consideration that the voxel data contain the volume fractions of fluid and solid, a VOF function [22] is introduced to describe the multi-component geometry. Further, the left Cauchy-Green deformation tensor [23], which quantifies a level of solid deformation, is introduced on each grid point and temporally updated to describe a Mooney-Rivlin law [24, 25]. The method does not restrict the particle Reynolds number range as long as the cell Reynolds number is of the order unity or less. It has been demonstrated significant advances in our understanding of the geometrical flexibility [16,18].

In the present paper, firstly, we will outline the basic equations of the system consisting of Newtonian fluid and hyperelastic material, and how to implement the given voxel-based geometry into the code. Secondly, we will explore the validity of the advocated numerical method. Thirdly, we will demonstrate three-dimensional motions of biconcave neo-Hookean particles in a Poiseuille flow.

NOMENCLATURE

B left Cauchy-Green deformation tensor.
c_1, c_2 moduli of elasticity.
D strain rate.
I unit tensor.
L velocity gradient tensor.
p pressure.
t time
v velocity vector.

Symbols
ϕ volume fraction.
μ viscosity.
ρ density.
$\boldsymbol{\tau}$ deviatoric Cauchy stress tensor.

Subscripts
f fluid phase.
s solid phase.
0 initial state.

Superscripts
T transpose
$'$ deviatoric part of second-order tensor.

BASIC EQUATIONS

Governing equations

The fluid and solid are assumed to be incompressible and to possess the same density. We use one set of governing equations for the whole flow field, which is one of the standard ways in multiphase flow simulations, and known as a one-fluid formulation [26]. The mass and momentum conservations are

$$\nabla\cdot\mathbf{v} = 0, \tag{1}$$

$$\rho\left(\partial_t\mathbf{v} + \mathbf{v}\cdot\nabla\mathbf{v}\right) = -\nabla p + \nabla\cdot\boldsymbol{\tau}, \tag{2}$$

where the deviatoric Cauchy stress stress $\boldsymbol{\tau}$ is modeled in the subsequent subsection.

Constitutive equations

The constitutive equations are described on an Eulerian frame adjusted to the voxel-based geometry. The fluid and solid phases are distinguished by the volume fraction of solid ϕ_s, which obeys

Copyright © 2011 by JSME

Downloaded From: https://proceedings.asmedigitalcollection.asme.org on 06/30/2019 Terms of Use: http://www.asme.org/about-asme/terms-of-use

$$\partial_t \phi_s + \mathbf{v}\cdot\nabla\phi_s = 0. \tag{3}$$

We assume that fluid is Newtonian, and the solid stress has both the elastic and viscous components. The deviatoric Cauchy stress $\boldsymbol{\tau}$ is written in a mixture form

$$\boldsymbol{\tau} = 2(1-\phi_s)\mu_f \mathbf{D}' + \phi_s\left\{2c_1\mathbf{B}' + 2c_2(\mathrm{tr}(\mathbf{B})\mathbf{B}' - (\mathbf{B}\cdot\mathbf{B})') + 2\mu_s\mathbf{D}'\right\}, \tag{4}$$

where c_1, and c_2 denote the moduli of elasticity of a linear Mooney-Rivlin material, and $\mathbf{D} = (\nabla\mathbf{v} + \nabla\mathbf{v}^T)/2$ the strain rate. The prime on the second-order tensor stands for the deviatoric tensor, namely, $\mathbf{T}' = \mathbf{T} - \mathrm{tr}(\mathbf{T})\mathbf{I}/3$ for a tensor $\mathbf{T}$. To avoid the numerical instability stemming from a rather rough distribution of $\mathbf{B}$ in the fluid region [13, 18], we introduce a modified deformation tensor $\tilde{\mathbf{B}}$ to be zero in the fluid region:

$$\tilde{\mathbf{B}} = \begin{cases} \phi_s^{1/2}\mathbf{B} & \text{for} \quad \phi_s \geq \phi_{\min}, \\ 0 & \text{for} \quad \phi_s < \phi_{\min}. \end{cases} \tag{5}$$

The second term in the right-hand-side of (4) immediately reads

$$2\phi_s^{1/2}c_1\tilde{\mathbf{B}}' + 2c_2(\mathrm{tr}(\tilde{\mathbf{B}})\tilde{\mathbf{B}}' - (\tilde{\mathbf{B}}\cdot\tilde{\mathbf{B}})') + 2\phi_s\mu_s\mathbf{D}'.$$

The left Cauchy-Green deformation tensor obeys

$$\partial_t\tilde{\mathbf{B}} + \mathbf{v}\cdot\nabla\tilde{\mathbf{B}} - \mathbf{L}\cdot\tilde{\mathbf{B}} - \tilde{\mathbf{B}}\cdot\mathbf{L}^T = 0, \tag{6}$$

where $\mathbf{L}(=\nabla\mathbf{v})$ denotes the velocity gradient tensor.

General descriptions of numerical methods

The basic equations are directly solved by means of the finite difference method using a uniform mesh. All the spatial derivatives are approximated by the second-order central difference scheme on a staggered grid [27], except the advection terms in (3) and (6) solved by the fifth-order WENO method [28, 29]. To integrate the equations in time, we employ the second-order Adams-Bashforth and Crank-Nicolson schemes. To complete the time marching in the momentum equation (2) and to simultaneously satisfy the solenoidal condition (1), we employ the SMAC procedure [30] by solving a Poisson equation for the pressure. For a more detailed description, we refer the readers to [18].

The solid volume fraction ϕ_{s0} at the starting point is given as a set of artificial voxel data. As a preprocessing, we numerically compute the ratio of the occupied solid to each control volume from the initial configuration of the system geometry, and construct the distribution of ϕ_{s0}.

VALIDATION TESTS

A solid motion in a lid-driven cavity flow

We made a comparison with well-validated FSI analysis [18]. We perform full Eulerian simulations of deformable solid motion in a lid-driven cavity with the same setup and conditions as in [31], in which a mixed Lagrangian and Eulerian approach was employed. The initial setup is schematically illustrated in figure 1(a). The size of the cavity is $L_x \times L_y = 1\times 1$. The cavity is bounded by rigid walls. Initially, the system is at rest. The unstressed solid shape is circular with a radius of 0.2, and centered at (0.6, 0.5). At t = 0, to drive the fluid and solid motions, the top wall starts to move at a speed of V_W = 1 in x direction. The material properties are ρ = 1, μ_f = $\mu_s = 10^{-2}$, c_1 = 0.05 and c_2 = 0.

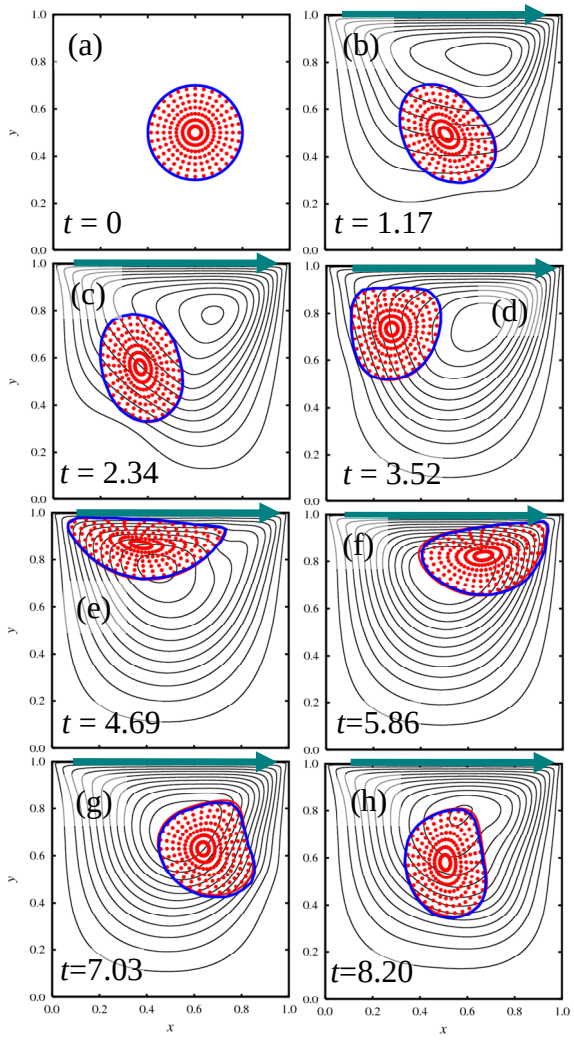

FIGURE 1. COMPARISON OF THE SOLID DEFORMATION IN THE LID-DRIVEN FLOW WITH THE AVAILABLE SIMULATION RESULTS [31].

Copyright © 2011 by JSME

Downloaded From: https://proceedings.asmedigitalcollection.asme.org on 06/30/2019 Terms of Use: http://www.asme.org/about-asme/terms-of-use

Figure 1 visualizes the particle deformation and the streamlines for eight consecutive time instants. The solid curves correspond to the particle outlines obtained in [31]. The dotted points correspond to the material points inside the particle predicted by the present full Eulerian simulation with a mesh 1024×1024. These are tracked just to transfer images of the particle deformation, but we did not use these material points for computing solid stress and strain. The particle moves and deforms driven by the fluid flow, and exhibits highly deformed shape when the particle approaches the wall. It should be noticed that no special artifact for avoiding a particle-wall overlap is implemented into the present method because the particle-wall hydrodynamic repulsion is likely to be brought due to the geometry change via the particle deformation. The solid shapes predicted by the present Eulerian simulation are in excellent agreement with the well-validated results in [31].

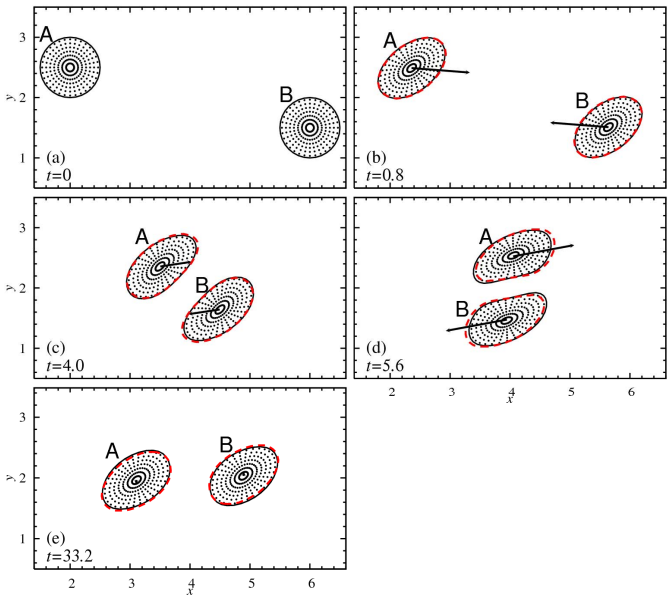

FIGURE 2. COMPARISON OF THE PARTICLE-PARTICLE INTERACTION WITH THE AVAILABLE SIMULATION RESULTS [32].

Two particles interaction in a Couette flow

Further, we made a comparison [18] with the available numerical analysis of the interaction between two deformable particles in a Couette flow performed in [32], in which the ALE approach was employed. The computational extent is $L_x \times L_y = 8\times4$. Initially, the system is at rest. Two unstressed solid particles are initially circular with a radius of 0.5, and centered at $\mathbf{x}_{c,A}$ = (2, 2.5) and $\mathbf{x}_{c,B}$ = (6, 1.5) as depicted in figure 2(a). The upper and lower plates located at y = 4 and y = 0, respectively, start to move impulsively to drive the fluid and solid motions at speeds of $V_W^{\text{upper}} = 1$ and $V_W^{\text{lower}} = -1$ in x direction. The no-slip condition is imposed on the plates, while the periodic condition is applied in x direction. The material properties are ρ = 1, μ_f = 20, μ_s = 0, c_1 = 0 and c_2 = 40.

Figure 2 visualizes the two-particle shape for five time instants. The dotted markers are, again, to represent the solid deformations in the present full Eulerian simulation with a mesh 1024×512. The arrows at the particle centers are the instantaneous translating velocity vectors. The dashed curves in figure 2 correspond to the outlines of the particles obtained in [32]. As examined in [32], the particles experience somehow complicated interactions involving the "roll over"' and "bounce back" modes even in such a simple system. The solid shape obtained by the present Eulerian simulation is again in agreement with the well-validated result [32], indicating that the particle-particle interaction is also reasonably captured by the present approach.

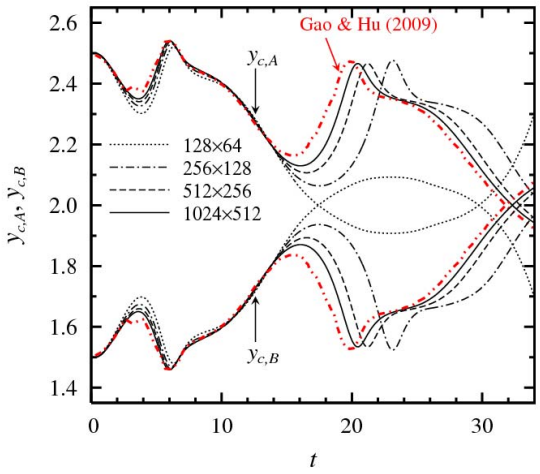

FIGURE 3. TEMPORAL EVOLUTION OF PARTICLE y_c-POSITION FOR VARIOUS NUMBER OF GRID POINTS. COMPARISON WITH THE RESULTS IN [32].

Figure 3 shows the temporal evolution of the y_c-position of the particle centroid for various grid resolutions ($N_x \times N_y = 128\times64, 256\times128, 512\times256, 1024\times512$). In the ALE computation [32], the finite element mesh is refined within the particle-particle gap, whereas in the present Eulerian simulation, the grid size is uniform and fixed. When the plot shows peaks around t = 3, t = 16 and t = 20, the gap between the particles is narrow, and the particle undergoes relatively strong hydrodynamic force owing to a squeezing effect. Such a narrow-gap effect is less resolved by the present method than the full Lagrangian method especially for the low spatial resolution cases, that is reflected on the larger deviations from the result in [32] preferentially at the peaks. In the higher spatial resolution, the profiles of the present simulation get closer to the ALE result [32].

Copyright © 2011 by JSME

Downloaded From: https://proceedings.asmedigitalcollection.asme.org on 06/30/2019 Terms of Use: http://www.asme.org/about-asme/terms-of-use

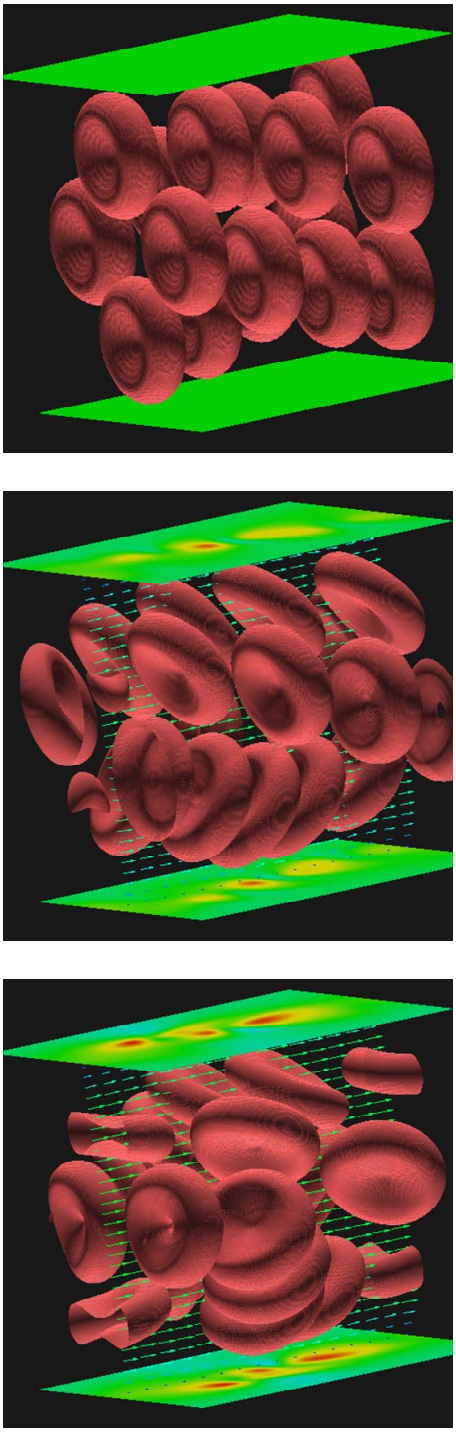

FIGURE 4. SNAPSHOTS OF DISCOID BICONCAVE PARTICLES OF THE NEO-HOOKEAN MATERIAL IN A POISEUILLE FLOW. THE TOP (a), MIDDLE (b), AND BOTTOM (c) PANELS SHOW THE PARTICLE INTERFACES AT t = 0, t = 5, AND t = 20, RESPECTIVELY. THE COLOR ON THE WALLS INDICATE THE SHEAR STRESS

BICONCAVE PARTICLES IN A POISEUILLE FLOW

One of the strong advantage of the present simulation method is characterized by no process of generation and reconstruction of the unstructured meshes. The use of the Eulerian method makes it easily possible to perform a FSI simulation even on a target with a complicated geometry, if the distribution of the solid volume fraction at the starting point is provided. As examples of the Eulerian analyses, three-dimensional interactive motions of several neo-Hookean discoid biconcave particles, which replicate the shape of RBC, in Poiseuille flows are demonstrated.

The initial and neutral shape of the particle is biconcave. Following [33], we describe the initial interface of the particle, of which the centroid is located at (x_c, y_c, z_c), together with a characteristic length a, as

$$\frac{x-x_c}{a}=\pm\frac{1}{2}\left(b_1+b_2\sigma+b_3\sigma^2\right)\sqrt{1-\sigma}, \tag{7}$$

with the coefficients b_1 = 0.207, b_2 = 2.003, and b_3 = –1.123. We set to $\sigma=\{(y-y_c)^2+(z-z_c)^2\}/a^2$. The system is bounded by the bottom (y = 0) and top ($y = L_y$) plates, and is periodic in x and z directions with the periodicity of L_x and L_z, respectively . Initially, the system is at rest. To pump the fluid and solid, the uniform pressure gradient $-\Delta P/L_x$ is applied to the system for the time $t\geq 0$. The system is supposed in stationary equilibrium before the driving pressure is imposed. The size of the computational domain is $L_x\times L_y\times L_z=7.2\times 7.2\times 7.2$ with the number of grids of $128\times128\times128$. The particle characteristic length is a = 1.36, and the driving pressure gradient is $-\Delta P/L_x=1$. Initially, 16 unstressed particles are seeded in the system as shown in Figure 4(a). Temporal evolution of the particle position and orientation is shown in Figure 4. The particles deform and translate in the downstream. As the time goes on, they rotate and tend to be more mixed.

To check whether the an conservation is correctly captured by the present numerical method, we examine a budget of the overall kinetic-energy transport written as

$$I-\varepsilon_s-\varepsilon_f-\frac{\mathrm{d}E}{\mathrm{d}t}=0, \tag{8}$$

where $I(=\langle v_x(-\Delta P/L)\rangle_V)$, $\varepsilon_s(=\langle\phi_s G\mathbf{B}':\mathbf{D}'\rangle_V)$, $\varepsilon_f(=\langle 2\mu\mathbf{D}':\mathbf{D}'\rangle_V)$, and $E(=\langle\rho\mathbf{v}\cdot\mathbf{v}\rangle_V/2)$ (here, $\langle ...\rangle_V$ stands for the average over the entire domain) denote the energy input rate, the strain energy rate, the energy dissipation rate, and the kinetic-energy, respectively. Figure 5 shows the time history of each contribution in the left-hand-side of (8). The double-chained curve in Fig. 5 shows the summation of the left-hand-side terms of (8). Its absolute value is much smaller than the variation of the contributions of the individual terms. Therefore, the system is well conserved during the simulation in view of the energy balance, and the energy exchange between the fluid and solid phases via the solid deformation is reasonably guaranteed.

Copyright © 2011 by JSME

Downloaded From: https://proceedings.asmedigitalcollection.asme.org on 06/30/2019 Terms of Use: http://www.asme.org/about-asme/terms-of-use

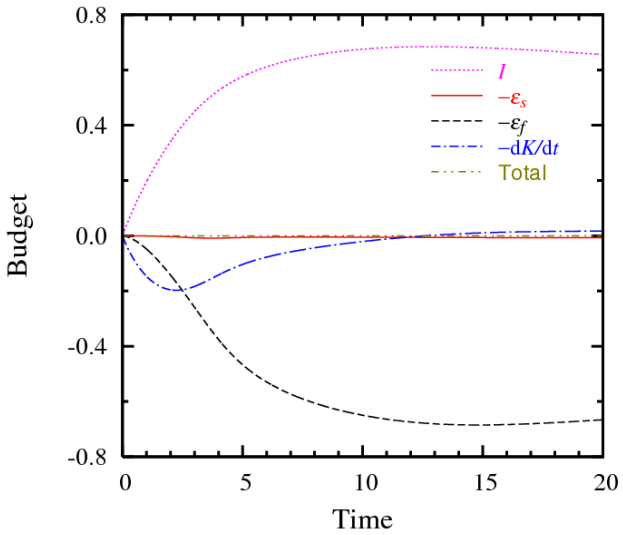

FIGURE 5. THE BUDGET OF THE KINETIC-ENERGY TRANSPORT IN THE POISEUILLE FLOW CONTAINING 16 NEO-HOOKEAN PARTICLES.

CONCLUSION AND PERSPECTIVES

A full Eulerian simulation method for solving Fluid-Structure Interaction (FSI) problems has been developed. It is suitable for the voxel data, which are converted from the medical CT/MRI image and describe multi-component geometry. It releases the coupling simulation from the mesh generation procedure. The present study demonstrated the validity of the simulation method, which consistently captured the well-validated simulation data for the deformed solid motion in the lid-driven cavity [31] and for two particles interaction in the Couette flow [32]. To demonstrate the feasibility in dealing with a system involving multiple bodies, the present Eulerian method was applied to three-dimensional motions of 16 discoid biconcave neo-Hookean particles in the Poiseuille flow.

If the distribution of the solid volume fraction for the initial geometry is given, the present approach facilitates to solve the FSI problem. It provides a significant boost of the geometrical flexibility, and thus encourages one to tackle a target with a complicated geometry. A characteristic of the Eulerian analysis is to make it easily possible to perform a coupled analysis using general computational algorithms for incompressible fluid. In consideration of a fact that a large-scale computation is essential when a realistic system is analyzed, the expertise for parallelization that has been cultivated in the field of the computational fluid dynamics can be utilized, which would be a large advantage in the realization of massively parallel computation. The expansion of the scale and models allows us to analyze a series of phenomena starting from the adsorption, under a condition in which many red blood cells are present, and would gain insight into the dynamics in thrombosis.

To improve the accuracy in the fluid-structure coupling, the ideas of the immersed interface treatment [34, 35] and the localized strain formulation [36] would be effective. It is a challenging task to overcome the multiphysics difficulty particularly associated with the difference in constitutive laws for fluid and solid. The sharp interface-capturing and the robust time advancement are the ongoing subject.

ACKNOWLEDGMENTS

This research was supported by Research and Development of the Next-Generation Integrated Simulation of Living Matter, a part of the Development and Use of the Next-Generation Supercomputer Project of the Ministry of Education, Culture, Sports, Science and Technology (MEXT), and by the Grant-in-Aid for Young Scientist (B) (No.21760120) of MEXT.

REFERENCES

[1] Taylor, C.A., Hughes, T.J.R. and Zarins, C.K., 1998. “Finite element modeling of blood flow in arteries,” *Comput. Methods. Appl. Mech. Engrg.*, **158**, pp. 155–196.

[2] Torii, R., Oshima, M., Kobayashi, T. and Takagi, K., 2001. “Numerical simulation system for blood flow in the cerebral artery using CT imaging data,” *JSME Int. J. Ser. C*, **44**, pp. 982–989.

[3] Hirt, C.W., Amsden, A.A. and Cook, J.L., 1974. “An arbitrary Lagrangian-Eulerian computing method for all flow speeds,” *J. Comput. Phys.*, **14**, pp. 227–253.

[4] Hughes, T.J.R., Liu, W.K. and Zimmermann, T.K., 1981. “Lagrangian-Eulerian finite element formulation for incompressible viscous flows,” *Comput. Methods Appl. Mech. Engrg.*, **29**, pp. 329–349.

[5] Tezduyar, T.E., Behr, M. and Liou, J., 1992. “A new strategy for finite element computations involving moving boundaries and interfaces - the deforming-spatial-domain/space-time procedure: I. The concept and the preliminary numerical tests,” *Comput. Methods Appl. Mech. Engrg.*, **94**, pp. 339–351.

[6] Tezduyar, T.E., Behr, M., Mittal, S. and Liou, J., 1992. “A new strategy for finite element computations involving moving boundaries and interfaces - the deforming-spatial-domain/space-time procedure: II. Computation of free-surface flows, two-liquid flows, and flows with drifting cylinders,” *Comput. Methods Appl. Mech. Engrg.*, **94**, pp. 353–371.

[7] Peskin, C.S., 1972. “Flow patterns around heart valves: a numerical method,” *J. Comput. Phys.*, **10**, pp. 252–271.

[8] Peskin, C.S., 2002. “The immersed boundary method,” *Acta Numerica*, **11**, pp. 479–517.

[9] Zhang, L., Gerstenbetger, A., Wang, X. and Liu, W.K., 2004. “Immersed finite element method,” *Comput. Methods Appl. Mech. Engrg.*, **193**, pp. 2051–2067.

Copyright © 2011 by JSME

Downloaded From: https://proceedings.asmedigitalcollection.asme.org on 06/30/2019 Terms of Use: http://www.asme.org/about-asme/terms-of-use

[10] Matsunaga, N., Liu, H. and Himeno, R., 2002. "An immersed-based computational fluid dynamics method for haemodynamic simulation," *JSME Int. J. Ser. C*, **45**, pp. 989–996.

[11] Yokoi, K., Xiao, F., Lui, H. and Fukasaku, K., 2005. "Three-dimensional numerical simulation of flows with complex geometries in a regular Cartesian grid and its application to blood flow in cerebral artery with multiple aneurysms," *J. Comput. Phys.*, **202**, pp. 1–19.

[12] Van Hoogstraten, P.A.A., Slaats, P.M.A. and Baaijens, F.P.T., 1991. "A Eulerian approach to the finite element modelling of neo-Hookean rubber material," *Appl. Sci. Res.*, **48**, pp. 193–210.

[13] Liu, C. and Walkington, N.J., 2001. "An Eulerian description of fluids containing visco-elastic particles," *Arch. Rational Mech. Anal.*, **159**, pp. 229–252.

[14] Dunne, T., 2006. "An Eulerian approach to fluid-structure interaction and goal-oriented mesh adaptation," *Int. J. Numer. Meth. Fluids*, **51**, pp. 1017–1039.

[15] Cottet, G.-H., Maitre, E. and Milcent, T., 2008. "Eulerian formulation and level set models for incompressible fluid-structure interaction," *Math. Modelling and Numer. Anal.*, **42**, pp. 471–492.

[16] Sugiyama, K., Ii, S., Takeuchi, S., Takagi, S. and Matsumoto, Y., 2010. "Full Eulerian simulations of biconcave neo-Hookean particles in a Poiseuille flow," *Comput. Mech.*, **46**, pp. 147–157.

[17] Nagano, N., Sugiyama, K., Takeuchi, S., Ii, S., Takagi, S. and Matsumoto, Y., 2010. "Full-Eulerian finite-difference simulation of fluid flow in hyperelastic wavy channel," *J. Fluid Sci. Tech.*, **5**, pp. 475–490.

[18] Sugiyama, K., Ii, S., Takeuchi, S., Takagi, S. and Matsumoto, Y., 2011. "A full Eulerian finite difference approach for solving fluid-structure coupling problems," *J. Comput. Phys.*, **230**, pp. 596–627.

[19] Ii, S., Sugiyama, K., Takeuchi, S., Takagi, S. and Matsumoto, Y., 2010. "An implicit full Eulerian method for the fluid-structure interaction problem," *Int. J. Numer. Meth. Fluids*, (published online doi: 10.1002/fld.2460).

[20] Gilmanov, A. and Acharya, S., 2008. "A hybrid immersed boundary and material point method for simulating 3D fluid-structure interaction problems," *Int. J. Numer. Meth. Fluids*, **56**, pp. 2151–2177.

[21] Sugiyama, K., Nagano, N., Takeuchi, S., Ii, S., Takagi, S. and Matsumoto, Y., 2011. "Particle-in-cell method for fluid-structure interaction simulations of neo-Hookean tube flows," *Theor. Appl. Mech. Jpn.*, **59** (accepted).

[22] Hirt, C.W. and Nichols, B.D., 1981. "Volume of fluid (VOF) method for the dynamics of free boundaries," *J. Comput. Phys.*, **39**, pp. 201–225.

[23] Bonet, J. and Wood, R.D., 2008. '*Nonlinear Continuum Mechanics for Finite Element Analysis*,' Chap. 4, second edition, Cambridge University Press, Cambridge.

[24] Mooney, M., 1940. "A theory of large elastic deformation," *J. Appl. Phys.*, **11**, pp. 582–592.

[25] Rivlin, R.S., 1948. "Large elastic deformations of isotropic materials IV, Further development of general theory," *Phil. Trans. R. Soc. A*, **241**, pp. 379–397.

[26] Tryggvason, G., Sussman, M. and Hussaini, M.Y., 2007. "Immersed boundary methods for fluid interfaces," in Prosperetti, A. and Tryggvason, G. (Eds.), '*Computational Methods for Multiphase Flow*,' Chap. 3, Cambridge University Press, Cambridge.

[27] Harlow, F.H. and Welch, J.E., 1965. "Numerical calculation of time-dependent viscous incompressible flow of fluid with free surface," *Phys. Fluids*, **8**, pp. 2182–2189.

[28] Jiang, G.-S. and Shu, C.-W., 1996. "Efficient implementation of weighted ENO scheme," *J. Comput. Phys.*, **126**, pp. 202–228.

[29] Osher, S. and Fedkiw, R., 2003. '*Level Set Methods and Dynamic Implicit Surfaces*,' Chap. 3, Springer, New York.

[30] Amsden, A.A. and Harlow, F.H., 1970. "A simplified MAC technique for incompressible fluid flow calculation," *J. Comput. Phys.*, **6**, pp. 322–325.

[31] Zhao, H., Freund, J.B. and Moser, R.D., 2008. "A fixed-mesh method for incompressible flow-structure systems with finite solid deformation," *J. Comput. Phys.*, **227**, pp. 3114–3140.

[32] Gao, T. and Hu, H.H., 2008. "Deformation of elastic particles in viscous shear flow," *J. Comput. Phys.*, **228**, pp. 2132–2151.

[33] Gong, X., Sugiyama, K., Takagi, S. and Matsumoto, S., 2009. "The deformation behavior of multiple red blood cells in a capillary vessel," *J. Biomech. Engrg.*, **131**, 074504.

[34] LeVeque, R.J. and Li, Z., 1994. "The immersed interface method for elliptic equations with discontinuous coefficients and singular sources," *SIAM J. Numer. Anal.*, **31**, pp. 1019–1044.

[35] Li, Z. and Ito, K., 2006. '*The Immersed Interface Method*,' SIAM, Philadelphia.

[36] Okada, H. and Atluri, S.N., 1995. "Embedded localized strain zone constitutive model in finite strain and finite rotation," *Proc. of Int. Conf. on Computational Engineering Science*, pp. 2154–5159.

Copyright © 2011 by JSME

Downloaded From: https://proceedings.asmedigitalcollection.asme.org on 06/30/2019 Terms of Use: http://www.asme.org/about-asme/terms-of-use